Influence of Kinematic Hardening on Clinch Joining of Dual-Phase Steel HCT590X Sheet Metal

Johannes Friedlein, Julia Mergheim, and Paul Steinmann

Abstract Nowadays, clinching is a widely used joining technique, where sheets are joined by pure deformation to create an interlock without the need for auxiliary parts. This leads to advantages such as reduced joining time and manufacturing costs. On the other hand, the joint strength solely relies on directed material deformation, which renders an accurate material modelling essential to reliably predict the joint forming. The formation of the joint locally involves large plastic strains and possibly complex non-proportional loading paths, as typical of many metal forming applications. Consequently, a finite plasticity formulation is utilised incorporating a Chaboche–Rousselier kinematic hardening law to capture the Bauschinger effect. Material parameters are identified from tension–compression tests on miniature specimens for the dual-phase steel HCT590X. The resulting material model is implemented in LS-Dyna to study the locally diverse loading paths and give a quantitative statement on the importance of kinematic hardening for clinching. It turns out that the Bauschinger effect mainly affects the springback of the sheets and has a smaller effect on the joint forming itself.

Keywords Clinching · Material modelling · Kinematic hardening · Parameter identification · Bauschinger effect

J. Friedlein (✉) · J. Mergheim · P. Steinmann
Institute of Applied Mechanics, Friedrich-Alexander-Universität Erlangen-Nürnberg,
Egerlandstrasse 5, 91058 Erlangen, Germany
e-mail: Johannes.Friedlein@fau.de

J. Mergheim
e-mail: Julia.Mergheim@fau.de

P. Steinmann
e-mail: Paul.Steinmann@fau.de

Introduction

Clinching can be used to join sheet metal by pure deformation and eliminate the need for auxiliary joining parts, such as rivets or bolts. Consequently, the joint takes its strength purely from controlled local deformations leading to an interlock of both sheets. The formation of this interlock is relevant to predict the joint strength [1] and is related to severe plastic strains requiring reliable finite strain material models for finite element analyses. These constitutive models need to incorporate plastic hardening, where a distinction between isotropic and kinematic hardening is only important if non-proportional loading paths are present during the forming. Such loading paths can occur due to changing material flow directions as experienced by the successively oriented material flow during clinch joining. To quantitatively study the influence of kinematic hardening on clinch joining, we subsequently investigate two decisive factors as research questions (RQ): the material (RQ1) and the loading paths during the clinching process (RQ2).

Exemplarily, a *dual-phase steel HCT590X* is considered, which is often used in the automotive industry. It is well known that especially dual-phase steel can exhibit an early re-plastification and pronounced transition region at load reversal named Bauschinger effect [2, 3]. Due to the higher strength of dual-phase steel, it shows a stronger tendency for springback, which together with the microstructure combining soft and hard phases leads to larger Bauschinger effects compared to conventional steel [4, 5]. This has for instance been shown in [6] for the congeneric DP600 and similarly in [3, 5, 7]. By a sensitivity analysis for dual-phase steel [8], the most influential aspects of the Bauschinger effect have been identified as the transient hardening and yield stress at load reversal. Material modelling can capture the Bauschinger effect by kinematic hardening, which causes the yield surface to shift rather than increase in size as for isotropic hardening. To quantify the Bauschinger effect, cyclic tests can be conducted. This can be realised for instance by cyclic shearing [3], cyclic bending [7], or by tension–compression tests [7, 9]. Especially usually thin sheet metal is susceptible to buckling under compressive loading [7, 9]. Therefore, either special anti-buckling devices must be used [10] or miniature specimen are utilised as presented in [9] for tension–compression tests. Herein, the experiments are conducted at lower strains motivated by the observed stagnation of the Bauschinger effect towards larger strains [5]. Studies at various strain levels and pre-strain have been examined in [5, 6]. Herein, miniature tension–compression tests for sheet metal are conducted to investigate whether the steel HCT590X shows a Bauschinger effect (RQ1).

It has already been shown for several metal forming processes that kinematic hardening can have a significant influence on the final product. In deep drawing, for instance, the sheet is drawn over the intake radii causing an alternating plastification [2, 9], which is relevant for an accurate prediction of the springback. In addition to the springback at unloading, kinematic hardening might also affect the formation of

the interlock during the *clinch joining process*. This leads to the second research question to be addressed: Does clinch joining contain such non-proportional loading paths in the plastic region and is consequently influenced by kinematic hardening? (RQ2).

Material Modelling

The continuum mechanics framework is briefly presented in the following. It is important to note that the kinematics and the in LS-Dyna underlying balance equations are formulated in the geometrically nonlinear (finite strain) setup, whereas the herein used logarithmic strain space enables the material model to be formulated similarly as in the geometrically linear case.

Kinematics

A body in the reference (undeformed) configuration is described by its material points with coordinates X. The spatial (deformed) configuration contains the deformed body and its spatial coordinates x. Deformations of the body are captured by the nonlinear deformation map y as $x = y(X, t)$ and its gradient $F = \nabla_X y$.

Logarithmic Strain Space

The logarithmic strain space [11] is a hyperelastic-based approach that easily extends material models to the geometrically nonlinear setting. It has been successfully applied in various field, such as thermo-elastic–plastic solids [12] or additive manufacturing [13]. It is based on a modular geometric pre- and post-processing utilising the logarithmic Hencky strain.

The logarithmic Hencky strain H is part of Seth–Hill's family of generalised strain measures and can be computed from the right Cauchy–Green tensor $C = F^T \cdot F$ as

$$H = \frac{1}{2}\ln(C) = \sum_{a=1}^{3} \ln\left(\sqrt{\eta_a}\right) n_a \otimes n_a \tag{1}$$

and the three eigenvalues η_a and eigenvectors n_a of C [11].

Due to the properties of the tensor logarithm $\ln(\blacksquare)$, the Hencky strain is interpretable as a geometrically linear strain that can be handled as a small strain measure and applied as such. This enables material models to subsist inside the logarithmic strain space and be encompassed by the pre-processing of the strains in Eq. (1) and

a post-processing of the resulting logarithmic stress T and tangent(s) C back into the "real world". The latter concerns the (spatial) Cauchy stress σ and the Eulerian tangent E as

$$\sigma = T : \mathcal{P}^{\mathrm{E}}; \; E = \left[\mathcal{P}^{\mathrm{E}}\right]^{\mathrm{T}} : C : \mathcal{P}^{\mathrm{E}} + T : \mathcal{L}^{\mathrm{E}}, \tag{2}$$

derivable from the strain energy density with the Eulerian projection tensors $\mathcal{P}^{\mathrm{E}}$ and $\mathcal{L}^{\mathrm{E}}$ as stated for instance in [11]. The Fortran source code for the geometric pre- and post-processing is available online [14]. A Fortran tensor toolbox [15] is utilised for the implementation of the logarithmic strain space and the material model.

The benefits of the logarithmic strain space include its easy usability and wide applicability, whereas some limitations have recently been summarised [16].

Additive Plasticity with Combined Isotropic-Kinematic Hardening

The plastic material behaviour of the sheet metal is modelled by combined isotropic and kinematic hardening. This is described by an isotropic von Mises yield surface with classical isotropic hardening and a Chaboche–Rousselier type kinematic hardening [17]. Due to the use of the logarithmic strain space, the following material model is formulated similarly as a geometrically linear model.

The logarithmic stress T for additive plasticity can directly be computed from the total Hencky strain H with the bulk modulus κ, shear modulus μ, and symmetric plastic strain tensor H^{p}. The superscript dev denotes the deviatoric part of the tensor.

$$T(H) = \kappa \, \mathrm{trace}(H) I + 2\mu [H^{\mathrm{dev}} - H^{\mathrm{p}}] \tag{3}$$

Isotropic von Mises (J2-) plasticity with isotropic and kinematic hardening is assumed by the following yield condition and described by the scalar flow stress σ_{flow} and the second-order back stress tensor B, respectively.

$$\Phi^{\mathrm{p}} = \|T^{\mathrm{dev}} + B\| - \sqrt{2/3}\sigma_{\mathrm{flow}}\left(H^{\mathrm{p}}_{\mathrm{acc}}\right) \leq 0 \tag{4}$$

The additive framework can directly be extended to anisotropic plasticity, see for instance [11].

Isotropic hardening is introduced in the flow stress $\sigma_{\mathrm{flow}}\left(H^{\mathrm{p}}_{\mathrm{acc}}\right)$ either by a tabular true stress–strain curve or by an analytical hardening law as stated in Eq. (8).

The effect of kinematic hardening is incorporated into the yield function by the total back stress tensor B. Herein a Chaboche–Rousselier type kinematic hardening

model with multiple back stresses is chosen, which is expected to be well suited to describe the dual-phase steel [3, 6].

Starting from the yield function, the evolution equations for the internal variables, namely, the second-order plastic strain tensor H^p, the accumulated plastic strain H_{acc}^p, and the back stress tensors B_i are stated as

$$\dot{H}^p = \dot{\gamma} N; \ \dot{H}_{acc}^p = \sqrt{2/3}\|\dot{H}^p\| = \sqrt{2/3}\dot{\gamma}; \ \dot{B}_i = k_{1,i}\dot{\gamma} N - k_{2,i}\dot{\gamma} B_{n,i} \quad (5)$$

with the Lagrange multiplier $\dot{\gamma}$ and the evolution direction $N = [T^{dev} + B]/\|T^{dev} + B\|$. The evolution equations are integrated by an implicit Euler-Backward scheme

$$H_{n+1}^p = H_n^p + \gamma_{n+1}N; \ H_{acc\,n+1}^p = H_{acc\,n}^p + \sqrt{2/3}\gamma_{n+1} \quad (6)$$

and solved by a cutting-plane algorithm from [18]. The latter is chosen for simplicity and was found to fit well to the default BFGS solver in LS-Dyna. With the concept shown in [19] an arbitrary number of back stresses n_B can easily be introduced by summations resulting in the discrete incremental equation for the total back stress

$$B_{n+1} = \sum_{i=1}^{n_B} B_{n+1,i} = \sum_{i=1}^{n_B} \left[1 + k_{2,i}\gamma_{n+1}\right]^{-1} B_{n,i} + \gamma_{n+1}N \sum_{i=1}^{n_B} \frac{k_{1,i}}{\left[1 + k_{2,i}\gamma_{n+1}\right]} \quad (7)$$

Experiments and Parameter Identification

To study the Bauschinger effect and describe the combined isotropic-kinematic hardening behaviour, tension–compression tests are conducted. Together with uniaxial stress–strain curves, the material parameters are inversely identified.

Experimental Setup

Layer compression tests are conducted to determine the uniaxial stress–strain curve as outlined in [20, 21]. To distinguish between isotropic and kinematic hardening, tension–compression tests are utilised. For that purpose, miniature specimens are advantageous for sheet metal to avoid buckling under the compressive loading and thus eliminate the need for special anti-buckling devices [9]. The miniature specimen shown in Fig. 1a is clamped in a universal testing machine in Fig. 1b and loaded in a tension–compression-tension cycle (measured strain path in Fig. 2). At each load path change, the influence of the Bauschinger effect can be observed and used to distinguish between isotropic and kinematic hardening. The resulting force on the
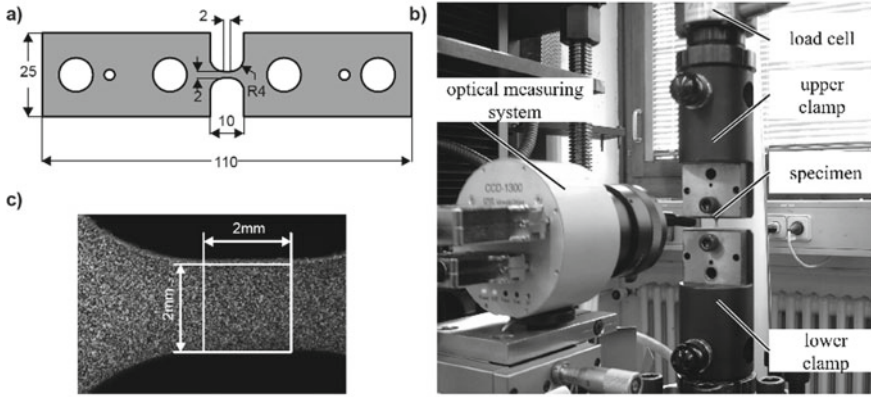
Fig. 1 Experimental setup of the tension–compression test. **a** specimen geometry and dimensions with sheet thickness of 1.5 mm. **b** experimental setup. **c** 2 × 2 mm measuring range (based on [9])

Fig. 2 Tension–compression-tension loading cycle. Optically measured true strain versus time response
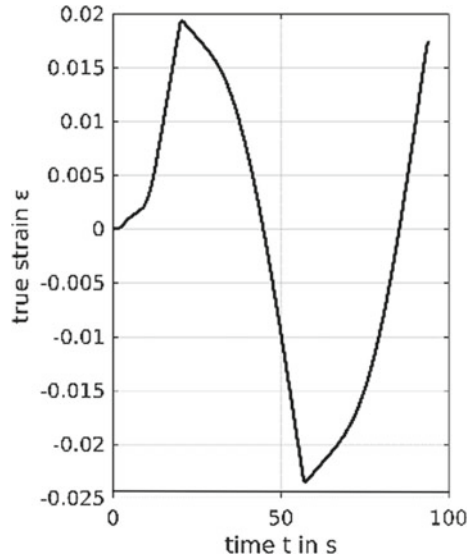
specimen is recorded by a load cell, whereas the deformation and the resulting strains in the measuring range (Fig. 1c) are determined optically.

Parameter Identification

For the steel HCT590X Young's modulus $E = 205800\,$MPa and Poisson's ratio $\nu = 0.3$ are chosen. In the following, the isotropic and kinematic hardening parameters are identified from layer compression tests and tension–compression tests.

Layer Compression Test

The flow curve of the considered steel HCT590X has already been identified from layer compression tests in [20], where this test method has been shown to be well suited for the subsequent application to clinching. The experimental results are plotted as true stress–strain data in Fig. 3 (red). This uniaxial flow curve is sufficient to either fit pure isotropic (IH) or pure kinematic hardening (KH).

For the description of *isotropic hardening*, particular points of the flow curve in Fig. 3 (red) could directly be used to describe the flow stress σ_{flow} in Eq. (4) by means of tabulated values. However, to be able to compare a pure isotropic and pure kinematic hardening model with the exact same uniaxial flow curve, the behaviour is described by an analytical ansatz

$$\sigma = \sigma_{\text{y}} + \sum_{i=1}^{n_Q} Q_i \big[1 - \exp(-b_i \cdot H_{\text{acc}}^{\text{p}}) \big] \tag{8}$$

which can exactly be matched by a Chaboche–Rousselier model with n_Q back stresses in Eq. (9) under monotonic uniaxial loading. By minimising the difference

Fig. 3 Uniaxial flow stress. Experimental results (red) determined from layer compression tests [20]. Isotropic (dashed), kinematic (dotted) and combined isotropic-kinematic (solid) are fitted to match the experimental results (red). Isotropic and kinematic hardening models are designed to exactly coincide under uniaxial loading

experiment (layer compression test, [20])
isotropic h.
pure kinematic h.
isotropic-kinematic h.
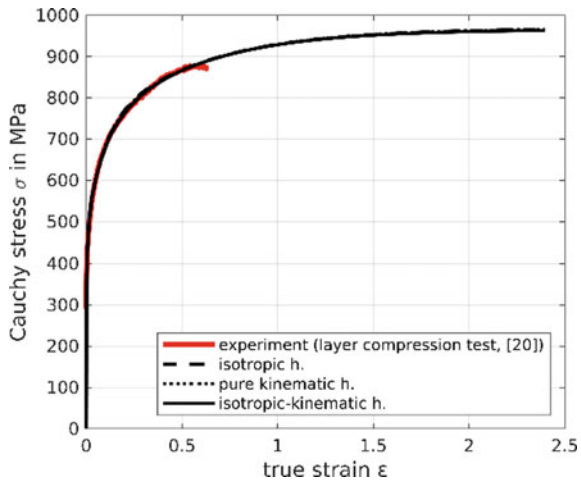
Table. 1 Plastic material parameters for isotropic and kinematic hardening

Behaviour	Symbol	Pure isotropic hardening (IH)	Pure kinematic hardening (KH)	Combined isotropic-kinematic hardening (IKH)	Unit
Yield stress	σ_y	371.32	371.32	337.91	MPa
Isotropic hardening	Q_1	257.42	–	260.55	MPa
	b_1	1.9030	–	1.9569	–
	Q_2	230.27	–	–	MPa
	b_2	12.020	–	–	–
	Q_3	111.22	–	–	MPa
	b_3	123.59	–	–	–
Kinematic hardening	$k_{1,1}$	–	326.58	33,333	MPa
	$k_{2,1}$	–	1.5538	1144.9	–
	$k_{1,2}$	–	1845.3	10,894	MPa
	$k_{2,2}$	–	9.8143	104.82	–
	$k_{1,3}$	–	9164.3	1490.3	MPa
	$k_{2,3}$	–	100.91	8.8490	–

between the experimental and numerical results, the material parameters are identified as stated in Table 1 considering an extrapolation to higher strains as suggested in [20]. As shown in Fig. 3, three summands ($n_Q = 3$) in Eq. (8) are sufficient to match the experimental flow curve (red).

On the other hand, the stress in loading direction for a pure *kinematic hardening* (KH) Chaboche–Rousselier model can be computed as

$$\sigma = \sigma_y + \sqrt{\frac{3}{2}} \sum_{i=1}^{n_B} \frac{k_{1,i}}{k_{2,i}} \left[1 - \exp\left(-\sqrt{\frac{3}{2}} k_{2,i} \cdot H_{acc}^p \right) \right] \tag{9}$$

From the comparison of Eq. (8) and (9), the parameters for KH, namely $k_{1,i}$ and $k_{2,i}$, can be determined from IH as

$$k_{1,i} = 2/3 \cdot Q_i \cdot b_i; \, k_{2,i} = \sqrt{2/3} b_i \tag{10}$$

if the same stress–strain curve is to be modelled with either pure isotropic or pure kinematic hardening. This ensures that all differences visible in the results between IH and KH can solely be attributed to load path changes and the fundamental difference between both hardening types.
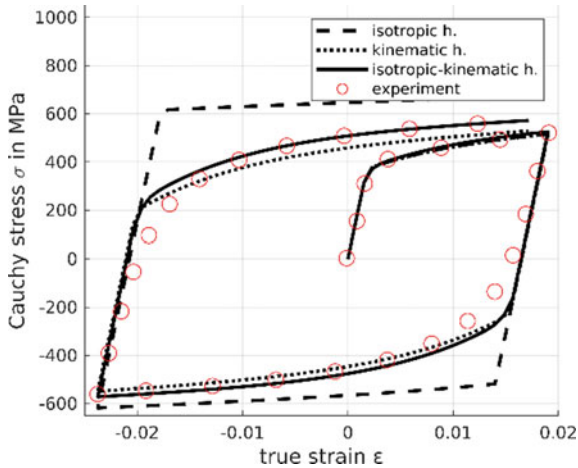
Fig. 4 True stress–strain results from tension–compression tests (red circles). Isotropic hardening (dashed) overestimates the yield stress at both load reversals. Pure kinematic hardening (dotted) underestimates the stress. Combined isotropic-kinematic hardening (solid) can model the response well

Tension–Compression Test

The tension–compression tests need to be considered to distinguish between isotropic and kinematic hardening. True stress–strain results from the former are depicted in Fig. 4. At each load reversal a distinctly earlier yielding and a transient area is visible that cannot be described by classical isotropic hardening (IH). On the other hand, pure kinematic hardening (KH) slightly underestimates the yield stress after each load reversal. Interestingly, even the KH model is not able to capture the extremely early re-yielding after the load reversal. This could, for instance, indicate an initial back stress from the previous manufacturing of the sheet metal included in [22].

Because of the (almost) uniaxial stress state in the tension–compression test, a 1D analytical model can be used to identify the parameters of the combined isotropic-kinematic hardening model (IKH) from the cyclic loading as listed in Table 1.

To sum up, Fig. 4 shows that the present HCT590X exhibits a pronounced Bauschinger effect (RQ1) and that the material model represents the experimental results for the layer compression test and tension–compression test sufficiently well.

Numerical Analysis of Clinch Joining

To analyse the influence of the Bauschinger effect on clinching, we firstly study the loading paths during the joining process. Only if non-proportional loading is present,
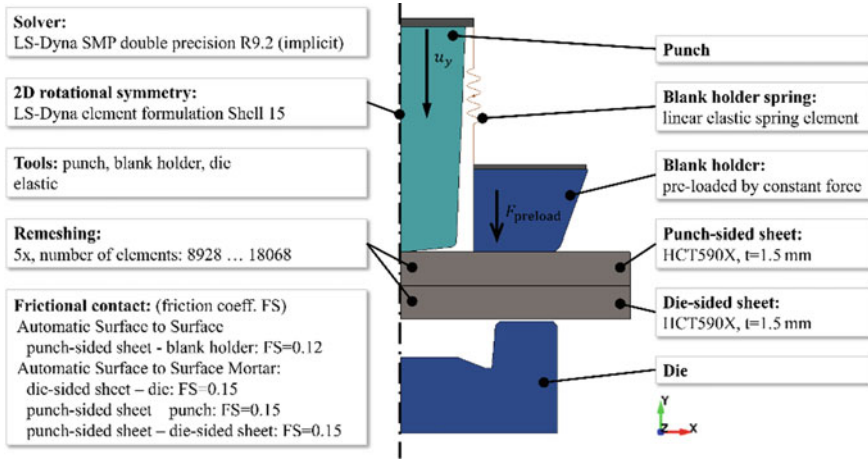
Fig. 5 Overview of the clinch joining process simulation in LS-Dyna (based on [23])

the different hardening types will be influential. Secondly, the results of clinching simulations with the hardening models from Table 1 are compared.

The clinch joining process is simulated in LS-Dyna (Solver: SMP, double precision, R9.2) as depicted in Fig. 5 with an implicit time integration. Rotational symmetry of the joint is utilised to reduce the model to 2D (axial symmetry, LS-Dyna element formulation Shell 15). The sheets are remeshed at predefined time intervals during the forming to avoid strong mesh distortion.

Loading Paths During Clinching

We propose to analyse the evolution of the Lode angle as a simple criterion to study the existence of non-proportional loading paths. The Lode angle parameter is defined in LS-Dyna as the normalised third deviatoric stress invariant [24]

$$\xi = \frac{27}{2} \frac{\det(\mathrm{dev}(\boldsymbol{\sigma}))}{\sigma^3} = (-1 \ldots 1) \quad \text{with} \quad \sigma_{\mathrm{vM}} = \sqrt{\frac{3}{2}} \|\boldsymbol{\sigma}^{\mathrm{dev}}\| \tag{11}$$

Proportional loading requires a constant Lode angle parameter ξ. However, a constant ξ does not guarantee a proportional loading, compare Fig. 6 where for instance up to 6 points on the initial yield surface (red circle) can possess the same ξ. But without erratic changes in the principal stress direction, the Lode angle parameter can be used to detect changes in the direction of the loading path. The latter can help to quantify the need for kinematic hardening during the process.

Figure 7 shows the evolution of the Lode angle parameter for three points in the sheets (points marked in Fig. 7d, at each remeshing the element that contains the tracer
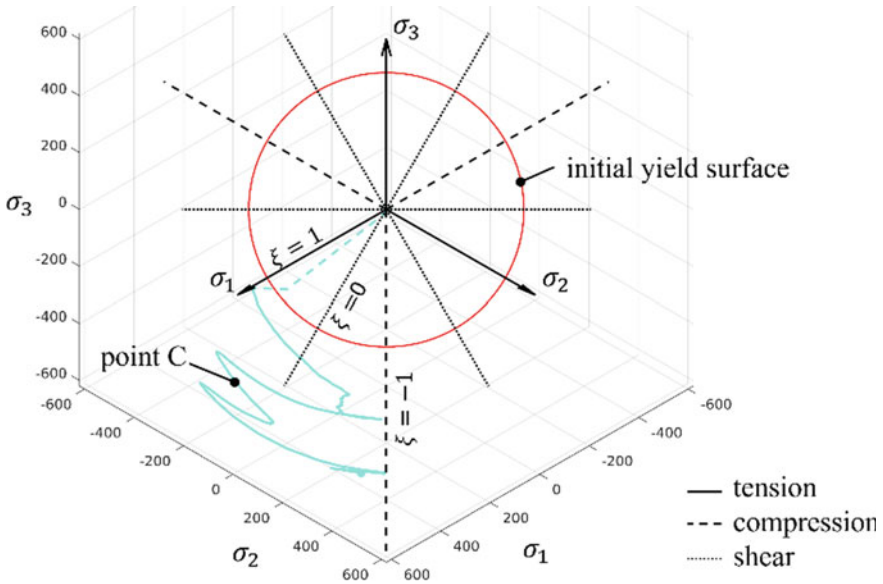
Fig. 6 Principal stress space viewed in the deviatoric plane. Along the positive principal directions (solid black lines) tension occurs ($\xi = 1$) and in negative direction compression (dashed black, $\xi = -1$). Pure shear ($\xi = 0$) is present along the bisectrices (dotted black). The principal deviatoric stress evolution for point C from Fig. 7c is exemplarily added (cyan)

point is selected). A finer discretisation with more remeshing steps than in Fig. 5 has been chosen for the stress analysis to improve the accuracy. Point A between the punch and the bottom of the die shows an almost constant evolution of the Lode angle parameter indicating a proportional loading at $\xi = -1$ (compression). In such areas, no differences between isotropic and kinematic hardening would be observed during loading. Points B and C detect changes in the Lode angle parameter indicating non-proportional loading paths. This is also visible for point C in Fig. 6 (cyan), where the stress state evolves radially due to the plastic hardening but also significantly shifts in tangential direction.

Consequently, we can summarise that the clinch joining process contains non-proportional loading paths (RQ2).

Influence of Kinematic Hardening

The three material parameter sets IH, KH and IKH listed in Table 1 are applied to the clinch joining simulation outlined previously. Figure 8 depicts the final geometry of the clinched joint for each model.

At first, Fig. 8 shows only larger differences in the springback of the two sheets on the right end. This is measured by the displacement of the upper-right corner (point
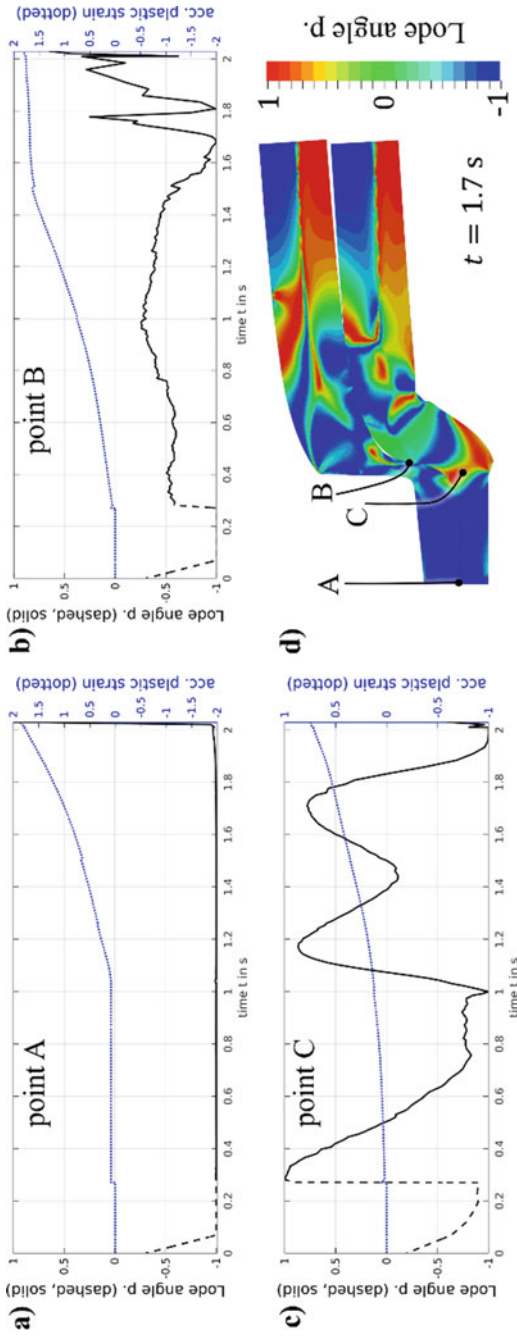
Fig. 7 Lode angle parameter ξ-evolution (solid black) for different points (A, B, C) in the sheets shown in (d) with their traces. **a** Point A resides between the punch and the bottom of the die. Thus, it undergoes compression ($\xi = -1$) remaining constant in the plastic region due to proportional loading. **b** Point B in the neck shows mainly a combination of compression and shear with some non-proportional evolution. **c** Point C undergoes substantial non-proportional loading including tension, shear and compression. Additionally, each figure shows the evolution of the accumulated plastic strain (H^p_{acc}, dotted blue). Only the ξ-evolution in the active plastic region (plastic strain rate $\dot{H}^p_{acc} > 0$) is relevant to trigger differences between isotropic and kinematic hardening, thus the elastic parts are marked by a dashed line. **d** Deformation of the sheets during the process at $t = 1.7s$ with the Lode angle parameter as colour map and the location and trace (black line) of the points A, B, and C
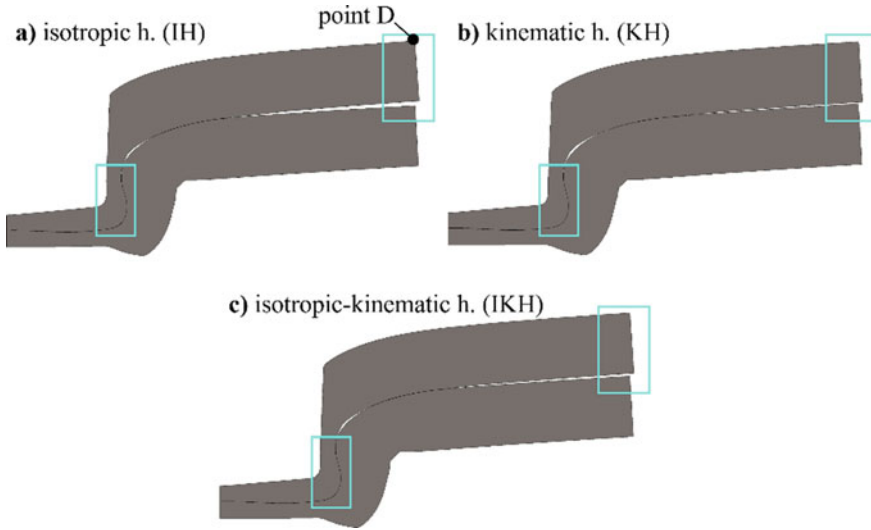
Fig. 8 Final geometry of the clinched joint for the different hardening models. Main differences are visible in the springback of the sheets on the right end and in the interlock region, as marked by the two rectangles and magnified in Fig. 11
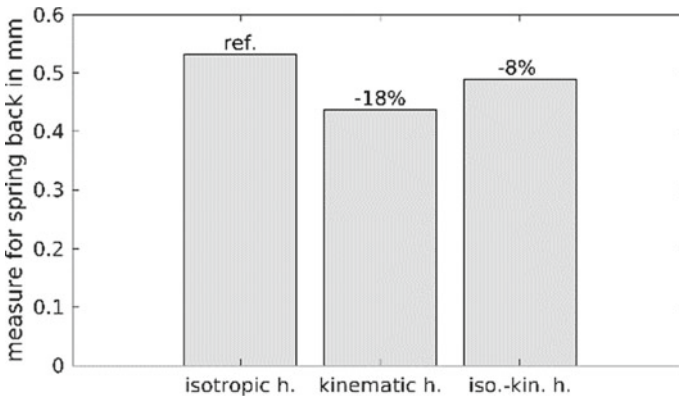

Fig. 9 Comparing the displacement of point D marked in Fig. 8a that can be used as a measure for the springback. With pure kinematic hardening the springback is reduced by about 18%

D marked in Fig. 8a) and compared in Fig. 9. By using a pure kinematic hardening model (KH), the final vertical deformation of point D is 18% lower than for the reference model with pure isotropic hardening (IH).

Secondly, changes in the interlock, as compared in Fig. 10, and neck shape are visible as depicted in Fig. 11. The interlock (defined in Fig. 11) is of high relevance for the joint strength [1] and appears to be also influenced by the hardening law.
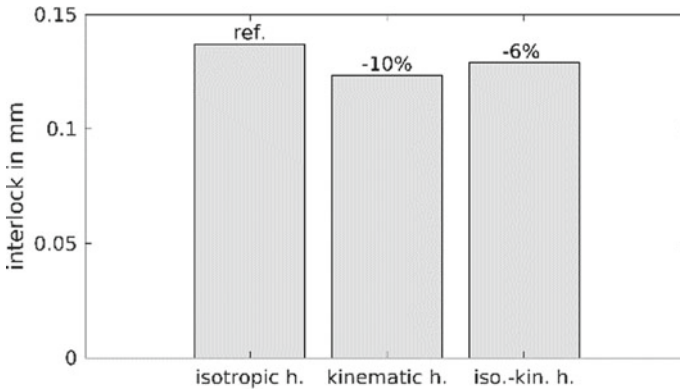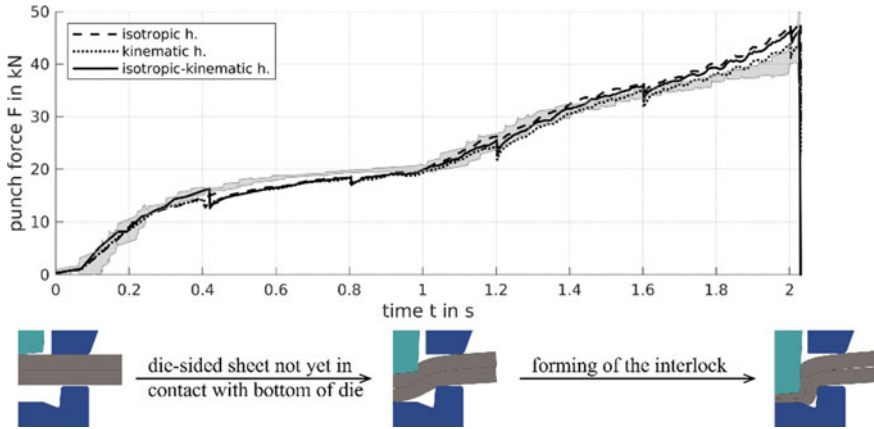
Fig. 10 Comparing the interlock for different hardening models. Kinematic hardening appears to reduce the formation of the interlock
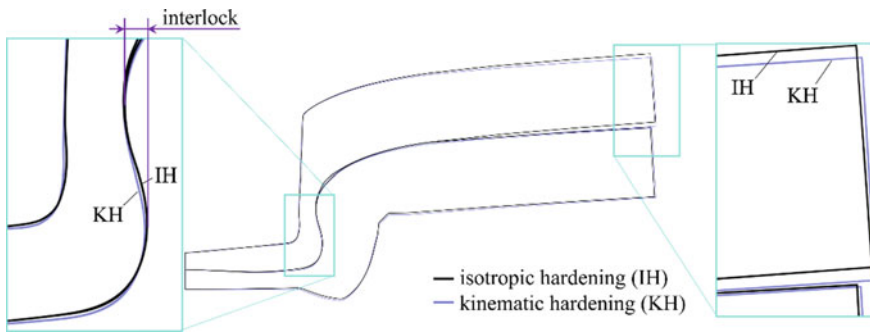
Fig. 11 Comparing the deformation of the clinched joint with isotropic (black, IH) and kinematic hardening (blue, KH). The right end of the sheet clearly shows a lower springback of the KH model. The zoom also reveals detectable differences in the formation of the neck and interlock

For both geometric quantities, the combined isotropic-kinematic hardening model settles in between IH and KH with differences of $(6\dots8)\%$.

Lastly, the process force, measured as the force on the punch, is compared for the three models in Fig. 12. Up to around $t = 1$s, the process forces between the three models are comparable. Once the die-sided sheet comes into contact with the bottom of the die to initiate the radial material flow that forms the interlock, differences in the process forces between the models become visible. In the end, isotropic hardening requires the highest punch force, whereas the pure kinematic hardening model remains approximately 6% lower. Exemplary experimental results for the punch force are added in grey in Fig. 12. Between $t = (0.4\dots1)$s the force is underestimated for each hardening model possibly due to deviations in the yielding or frictional behaviour, which is apparently not influenced by the hardening type.

Fig. 12 Comparing the punch force during the joint forming. The three different hardening models (line styles) show mainly differences during the secondary phase, namely the forming of the interlock, where kinematic hardening leads to lower process forces

Summary and Outlook

We have studied the plastification of dual-phase steel HCT590X sheet metal by miniature tension–compression tests. The resulting tension–compression-tension cycle enabled a distinction between isotropic and kinematic hardening completing the material model initially only defined by uniaxial flow curves from layer compression tests. Results indicate a pronounced Bauschinger effect (RQ1) as expected for the dual-phase steel. A Chaboche–Rousselier kinematic hardening model with multiple back stresses was implemented in LS-Dyna and equipped with the identified hardening parameters. Moreover, the loading paths during the clinch joining have been analysed. The evolution of the Lode angle parameter reveals that locally distinct non-proportional loading occurs (RQ2). Finally, the different hardening models have been applied to clinching simulations and their results compared. Kinematic hardening appears to primarily affect the final springback and only secondarily the joint forming and process force (RQ2). Future work could quantify the effect of kinematic hardening on the joint strength, for instance, by pull-out and shear tests. Even though the current material model was sufficient to study the fundamental influence of the Bauschinger effect on clinching, also more advanced kinematic hardening models could be utilised. The latter might be able to capture the observed early re-plastification that cannot be reproduced by a Chaboche–Rousselier model [2].

References

1. Roux E, Bouchard PO (2013) Kriging metamodel global optimization of clinching joining processes accounting for ductile damage. J Mater Process Technol 213(7):1038–1047
2. Banabic D (2010) Sheet metal forming processes: constitutive modelling and numerical simulation. Springer Science & Business Media, Berlin, Heidelberg
3. Yin Q et al (2012) A cyclic twin bridge shear test for the identification of kinematic hardening parameters. Int J Mech Sci 59(1):31–43
4. Zhonghua L, Haicheng G (1990) Bauschinger effect and residual phase stresses in two ductile-phase steels: Part I The influence of phase stresses on the Bauschinger effect. Metall Trans A 21(2):717–724
5. Weiss M et al (2015) On the Bauschinger effect in dual phase steel at high levels of strain. Mater Sci Eng A 643:127–136
6. Biallas A, Merklein M (2021) Material model for the production of steel fibers by notch rolling and fulling. Key Eng Mater 883:277–284
7. Eggertsen P, Mattiasson K (2011) On the identification of kinematic hardening material parameters for accurate springback predictions. Int J Mater Form 4(2):103–120
8. Zang S, Lee M, Kim JH (2013) Evaluating the significance of hardening behavior and unloading modulus under strain reversal in sheet springback prediction. Int J Mech Sci 77:194–204
9. Staud D (2010) Effiziente Prozesskettenauslegung für das Umformen lokal wärmebehandelter und geschweißter Aluminiumbleche. Ph.D. thesis, Friedrich-Alexander-Universität Erlangen-Nürnberg
10. Choi JS et al (2015) Measurement and modeling of simple shear deformation under load reversal: application to advanced high strength steels. Int J Mech Sci 98:144–156
11. Miehe C, Apel N, Lambrecht M (2002) Anisotropic additive plasticity in the logarithmic strain space: Modular kinematic formulation and implementation based on incremental minimization principles for standard materials. Comput Methods Appl Mech Eng 191(47–48):5383–5425
12. Aldakheel F (2017) Micromorphic approach for gradient-extended thermo-elastic–plastic solids in the logarithmic strain space. Contin Mech Thermodyn 29(6):1207–1217
13. Burkhardt C, Soldner D, Mergheim J (2020) A comparison of material models for the simulation of selective beam melting processes. Procedia CIRP 94:52–57
14. Friedlein J. Logarithmic_Strain_Space-Fortran. GITHUB. https://github.com/jfriedlein/Logarithmic_Strain_Space-Fortran. Accessed 1 March 2022
15. Dutzler A (2020) Tensor toolbox for modern Fortran - high-level tensor manipulation in Fortran. https://doi.org/10.5281/zenodo.4077378
16. Friedlein J, Mergheim J, Steinmann P (2022) Observations on additive plasticity in the logarithmic strain space at excessive strains. Int J Solids Struct 239–240:111416
17. Chaboche JL, Rousselier G (1983) On the plastic and viscoplastic constitutive equations—Part I: Rules developed with internal variable concept. J Pressure Vessel Technol 105(2):153–158
18. Simo JC, Hughes TJR (1998) Computational inelasticity. Springer Science & Business Media, New York
19. Wali M et al (2015) One-equation integration algorithm of a generalized quadratic yield function with Chaboche non-linear isotropic/kinematic hardening. Int J Mech Sci 92:223–232
20. Böhnke M et al (2021) Influence of various procedures for the determination of flow curves on the predictive accuracy of numerical simulations for mechanical joining processes. Mater Test 63(6):493–500
21. Friedlein J et al (2021) Inverse parameter identification of an anisotropic plasticity model for sheet metal. In: IOP Conf Ser: Mater Sci Eng 1157:012004
22. Marcadet SJ, Mohr D (2015) Effect of compression–tension loading reversal on the strain to fracture of dual phase steel sheets. Int J Plast 72:21–43
23. Bielak CR et al (2021) Numerical analysis of the robustness of clinching process considering the pre-forming of the parts. J Adv Join Proces 3:100038
24. Hallquist JO (2020) LS-DYNA Keyword User's Manual - vol II. Livermore Software Technology Corporation